The New Geological and Natural State Model of Hululais Geothermal Field

Sotarduga S. Nainggolan[1], Imam Prasetyo[1], Sardiyanto[1], Michael Gravatt[2], John O'Sullivan[2], and Karan Titus[3]

[1]PT. Pertamina Geothermal Energy Tbk, Grha Pertamina, Medan Merdeka Timur no 11-13, Jakarta, 10110, Indonesia
[2]Geothermal Institute, 70 Symonds Street, Auckland Private Bag 92019, Auckland 1142, Aotearoa New Zealand
[3]Sustainable Energy Research Group (SERG), University of Canterbury. 63 Creyke Road, Ilam, Christchurch 8041
ssj.nainggolan@pertamina.com

Keywords: *3D Geological Model, Numerical Simulation, Natural State*

ABSTRACT

Hululais Geothermal field, operated by PT Pertamina Geothermal Energy (PGE), is situated in the Province of Bengkulu, Sumatra Island, Indonesia. This volcanic-high terrain geothermal system is controlled by the Sumatra Fault System, which provides a high-enthalpy, liquid-dominated reservoir. As of 2025, the pre-exploitation phase is still underway in this field, with production scheduled to commence in the near future.

This paper aims to update the previous work by Nusantara et al. (2017) and Sisminardi (2019) by implementing the latest real subsurface datasets, hence yielding a well-constrained geological and natural state model of the Hululais field. Leapfrog geothermal software was used to create the three-dimensional geological model, while PyTOUGH coupled with AUTOUGH2 software was used to run the numerical simulations.

The geological model shows the lithology and stratigraphy sequences of the field, as well as the faults and alteration zone. The geological model was discretized and converted into the model grid for the numerical simulation. Temperature and pressure data acquired from previously conducted surveys were used for calibration. After extensive trial and error with manual calibrations, the natural-state model provided a satisfactory and reasonable temperature match. The average RMS error of the natural-state model is 15.1°C, meaning that 80% of the model is within 20°C difference with the downhole temperature.

The model shows that the high-temperature reservoir in the vicinity of well pads A, C, and E has a temperature of > 250 °C. In contrast, the lower temperature outflow zone lies in the vicinity of well pads B, D, P, and Q with a maximum temperature of 210°C. The temperature distribution also corresponds with the conceptual model, proving the relationship between the high-temperature upflow zone around Mount Beriti and Mount Gedang in the South with the lower temperature outflow zone in the Mount Cemeh area in the North.

1. INTRODUCTION

The Hululais field is located in the Lebong district, 60 km North of the city of Bengkulu-Indonesia. The total area of the concession is 2,836 km^2, which consists of three geothermal prospects: Hululais, Bukit Daun, and Tambang Sawah, as shown in Figure 1 (Pertamina Geothermal Energy, 2017b).

Hululais field is a high-terrain volcanic geothermal system and influenced by the Great Sumatra Fault system (Bambang et al., 2001). Two significant volcanoes controlling the geothermal systems are Mount Beriti (1910 masl) and Mount Gedang Hululais (2140 masl) (Geothermex, 2016), which are part of the Bukit Barisan Volcano Complexes. A local fault system in this field, typically with the orientation of its regional fault, trending NW-SE, is responsible for the distribution of surface manifestation (Koestono et al., 2015).

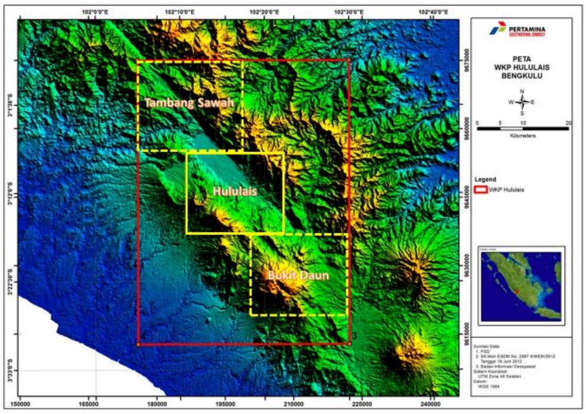

Figure 1: Map of Hululais geothermal field concession area.

2. GEOLOGICAL MODEL

The Hululais geological model is comprised of all relevant information ascertained from geology, geochemistry and drilling data. This allows a better understanding of the subsurface conditions and stratigraphic sequence in the key production area of the field. This data was collected from a combination of Pertamina Geothermal Energy's internal database and the previous work by Nusantara et al. (2017) and Sisminardi (2019) to yield the latest version of the model. The geological model aims to reconstruct the subsurface geological features and provide a basis for the development of the numerical model in Section 4 (Milicich et al., 2018).

In this study, Leapfrog Geothermal was used to build a geological model of Hululais. This software was developed by Seequent ltd explicitly for the geothermal industry.

2.1 Classifying the Lithology and Stratigraphy Sequent

There are seven types of lithology formation in the field, which sequentially from younger to older are; Lava Beriti Volcanic, Upper Beriti Volcanic, Lower Beriti Volcanic, Metasediment, Hululais Volcanic, Basement, and Granodiorite (Nusantara et al., 2017). Nevertheless, the basement rock is not found in the borehole data; it is added as a new horizon 200 m from the most bottomless well to accommodate the entire geothermal system. The rock formations are defined by petrographical analysis, X-ray

Proceedings 47th New Zealand Geothermal Workshop
11 -13 November 2025
Rotorua, New Zealand
ISSN 2703-4275

diffractometry, and fluid inclusion analysis to establish the similarity of each rock type (Nusantara et al., 2017).

To determine a reasonable size for the granodiorite intrusion, the high-density body from the geophysics-gravity model (Figure 2) is used to constrain the shape of granodiorite intrusion.

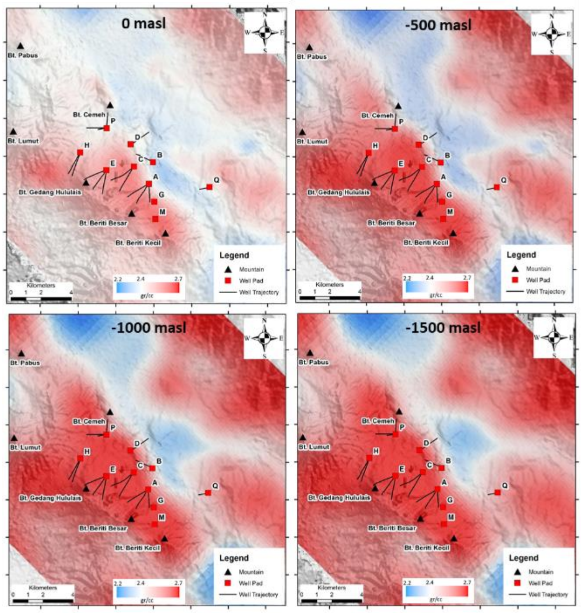

Figure 2: Horizontal slices at a various elevation of subsurface density in Hululais field (Pertamina Geothermal Energy, 2019b).

Moreover, the previous cross-section by (Nusantara et al., 2017) is imported to validate the new model. Figure 3 shows the data sets that have been used in developing the geological model.

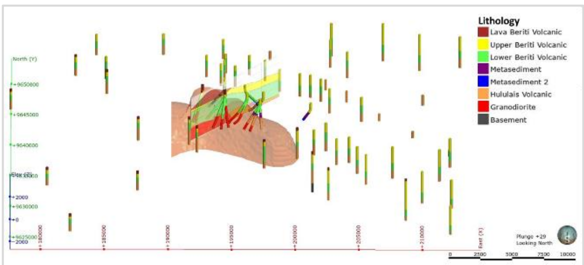

Figure 3: The distribution of 16 deviated actual wells, 56 vertical synthetic wells, cross-section, and the high-density gravity model.

2.2 Fault System

There are a series of faults that have an azimuth of NW-SW in the field, which are considered as the main faults as they control the lithology changes and the distribution of surface manifestations, thus indicating good permeability (Koestono et al., 2015). In addition to the major faults, there are also a series of minor faults, which have a direction perpendicular (NE-SW) to the main structure. Figure 4 shows the fault system in the geological model.

Faults can act as either high permeability pathways for flow or low permeability barriers of flow. The intersection of faults and lithologies is represented by the assignment of different rock types in the numerical model. This will allow greater control of the permeability structures, especially in the productive area of the system.

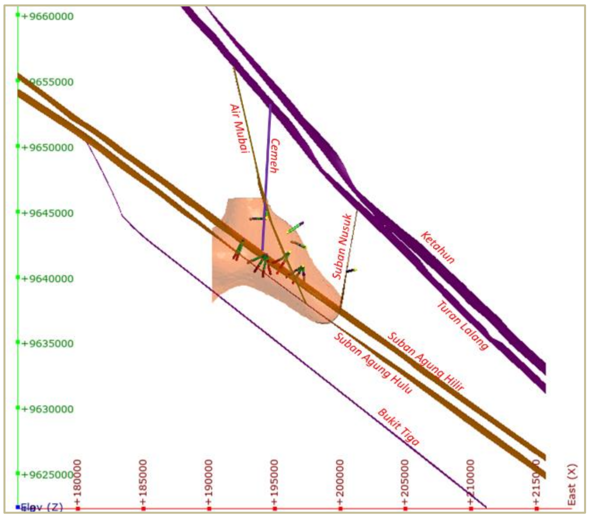

Figure 4: Fault system in the Hululais geological model.

2.3 Defining the Clay Cap

One of the tools to identify the clay cap distribution in a geothermal system is the geophysical magnetotelluric (MT) method since low resistivity rocks are closely linked with the impermeable clay cap (Cumming, 2009). The clay cap distribution in Hululais field is derived from the 3D MT-resistivity model (Figure 5). It has been confirmed that the 16 Ohm.m of the base conductor layer is associated with the argillic clay cap (Pertamina Geothermal Energy, 2019b). Moreover, the reservoir has a resistivity value of 60-120 Ohm.m while the resistivity of 16-60 ohm.m corresponds to the transition zone.

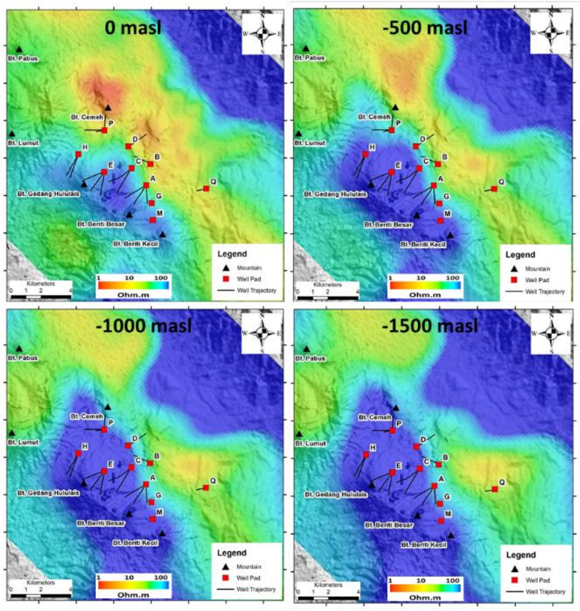

Figure 5: Horizontal slices of subsurface resistivity at various elevations in Hululais field.

After been loaded into the Leapfrog project, this geological and geophysical model was converted into a numerical model. The RBF interpolant technique is used to convert the 3D resistivity model into several isosurfaces body. As previously mentioned, clay cap in this field is represented as low-resistivity zone < 16 ohm.m, that corresponds with the resistivity logging data and the Methylene Blue test. Figure 6 visualizes the low-resistivity clay cap zone of the field.

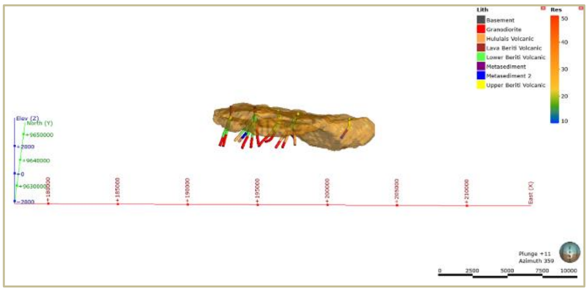

Figure 6: The low resistivity clay cap model of Hululais field.

The extent of the clay cap model is 13 km x 8 km NW-SE, which encompasses both production and reinjection wells. Moreover, the vertical thickness of the clay cap is about 1 km in the reservoir zone and up to 2 km in the marginal area. Furthermore, this clay cap body is considered to be Smectite/Illite clay, while bodies outside the clay cap are regarded as an unaltered zone, as shown in Figure 7.

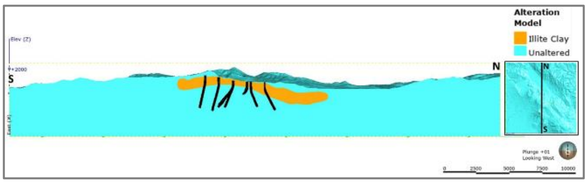

Figure 7: N-S vertical slice of the alteration model (projected wells are shown as a black line).

2.4 Integrated Geological Model

The final version of the model incorporates the clay cap as altered rocks of the corresponding lithologies. Furthermore, sections of faults intersecting the altered zone will be assigned different rock types. This will allow for additional control in this low permeability altered zone when calibrating the numerical model. This comprehensive version of the model can be seen in Figure 8.

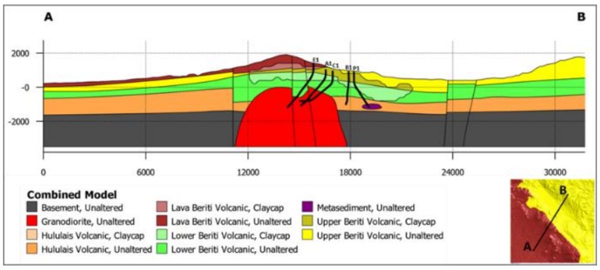

Figure 8: A-B Vertical slice of the geological model (projected wells are shown as a black line).

The vertical section (Figure 8) shows the stratigraphic lithology of the field. The formations are formed as a horizontal layer, honouring the cross-cutting relationship between each formation. The presence of the granodiorite intrusion and series of normal faults change the lateral distribution of the lithology, which results in unconformities within the model. The Granodiorite, which was encountered by wells E1, A1, and C1 intrudes the Basement, Hululais Volcanic, and part of the Lower Beriti Volcanic formation. The presence of faults in this intrusion rock increases the permeability and allows the deep thermal fluid to reach the reservoir (Nusantara et al., 2017). The clay cap can be found about 500 m above the Granodiorite, which intersects with part of Lower Beriti Volcanic, Upper Beriti Volcanic, and Lava Beriti Volcanic. This three-dimensional model, combining geology, faults, geophysics and the alteration zone, will later be discretized into a block model and used for the numerical model, which is explained in Section 4.

3. CONCEPTUAL MODEL OF HULULAIS GEOTHERMAL SYSTEM

The Hululais conceptual model was built by integrating the geology, geophysics, geochemistry, downhole temperature and well lithology. This model comprises the reservoir zone, upflow, outflow, recharge area, clay cap, and heat source location, as shown in Figure 9 and 10.

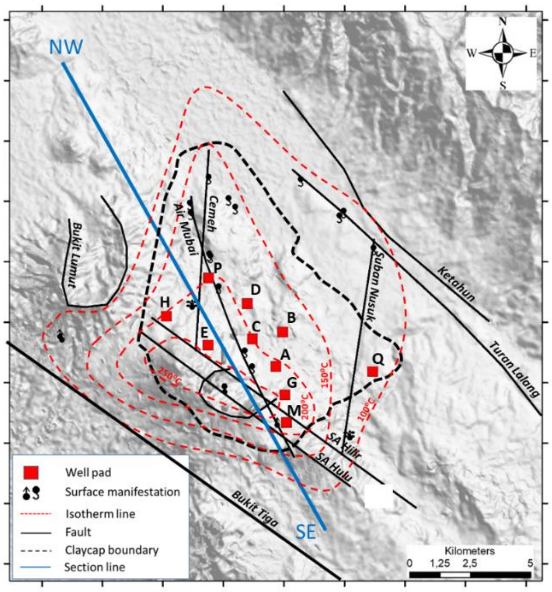

Figure 9: Top View of Hululais Geothermal System (NW-SE blue line is the vertical slice of the conceptual model).

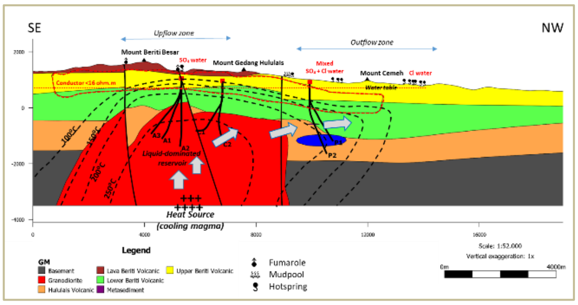

Figure 10: NW-SE section of Hululais conceptual model.

Hululais geothermal system is bounded by Turan Lalang fault in the North, Bukit Tiga fault in the South, Suban Nusuk fault in the East, and Bukit Lumut caldera in the West (Figure 9). The outside boundary of this geothermal system also associates with temperature < 100°C and warm springs of chloride water. The probable zone, which indicated by having temperatures > 225°C was estimated to have a total area of 25 km^2, while the most prospective zone, which is proven by well temperature data > 250°C has an area of 12 km^2 along the Suban Agung Hulu fault and Suban Agung Hilir fault.

An impermeable layer indicated by the <16 Ohm.m low-resistivity zone identified by the MT model and temperatures < 200°C extends to a shallow depth. This impermeable clay cap blocks the deep geothermal water from flowing up to the surface. However, the shape of the clay cap is poorly resolved in the South of Mount Beriti and Mount Gedang because of poor MT quality data in that area. The area below the clay cap, which corresponds with temperatures >200°C in the Lower Beriti Volcanic rock is the transition of the argillic and the propylitic alteration. This transition zone is associated with the top of the reservoir, that is marked by the occurrence of first epidote mineral (Pertamina Geothermal Energy, 2019b).

A cooling magma underlying Mount Beriti Besar and Mount Gedang (Figure 10), which is illustrated by a well-described collapse structure (Figure 9), appears to be a primary source for this geothermal system. This heat source is most likely underneath the volcanoes, as indicated by the high-elevation acid spring and fumarole (Geothermex, 2016). The presence of the upflow thermal manifestations corresponds with the Suban Agung Hulu fault and Subang Agung Hilir fault. These two faults are the sweet-spot when targeting the production well, as it offers high permeability and high temperature for the production wells (Pertamina Geothermal Energy, 2019b).

The upflow zone seems to be located in the vicinity of well pads A, C, E, G, and M, judging from the high-temperature zone, fumaroles and acid hot springs. From this upflow zone, the reservoir extends along the Granodiorite body. The liquid-dominated reservoir is shown as a high temperature zone with temperatures >250°C. The absence of well data to the south of Mount Beriti and Mount Gedang makes it unclear about how far the exploitable area of the thermal plume might extend in this region.

The presence of a mushroom shaped isotherm towards the N-W direction indicates a deep outflow of hydrothermal fluid. The reverse temperature profile can be found in well pad P, which indicates a cold downflow and the marginal area of the Hululais geothermal system. Moreover, the outflow of the system also links with chloride-water hot springs on the flank of Mount Cemeh. The occurrence of these surface manifestation complexes is possibly controlled by the Cemeh fault and Air Mubai fault, that allow the deep outflow of the geothermal fluid.

Well pad P, B, and D are situated in this outflow zone, however, according to the well testing result (Pertamina Geothermal Energy, 2019b) these wells have relatively poor permeability although they intersect the Air Mubai fault and Cemeh fault. The low permeability of these faults is possibly caused by silicification, as indicated by the silicified vein in the core samples of well pad D and P (Pertamina Geothermal Energy, 2019a). As a result, in order to satisfy the reinjection water requirements, eight wells were drilled from these two well pads (Pertamina Geothermal Energy, 2019b).

4. NUMERICAL MODELLING

In a numerical model, the subsurface is decomposed into several layers which comprise several irregular unstructured grid blocks. Each block in the model has its physical properties such as permeability, porosity, density, temperature, and pressure. In this project, the simulator used is AUTOUGH2 (Yeh, Croucher, & O'Sullivan, 2013), which is a modified version of TOUGH2 developed by the University of Auckland.

4.1 Geothermal Simulation Workflow

The conceptual model was built by incorporating various data sets such as geology, geophysics, geochemistry, pre-production field data, and production field data. These multidisciplinary data were integrated into a Leapfrog Geothermal project and then combined with PyTOUGH scripts and AUTOUGH2 to generate the two-way integration with the TOUGH2 numerical models (natural state model, production history model, and future scenarios) as illustrated in Figure 11 (Popineau et al., 2018). Hululais field is currently at the exploration stage, and hence no production history data acquired. As a result, in this research project, only natural state modelling was performed.

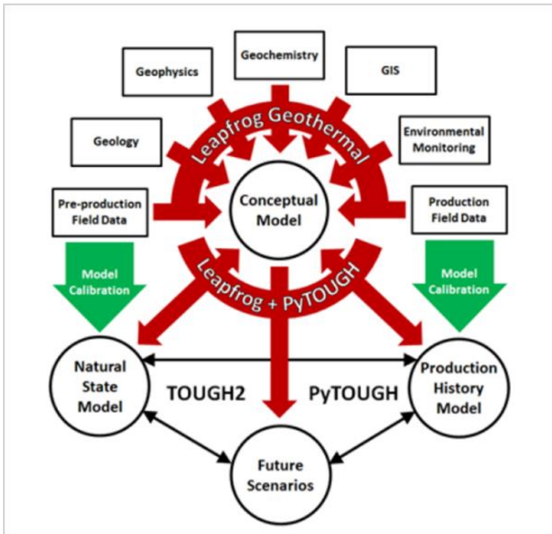

Figure 11: The geothermal modelling workflow using Leapfrog Geothermal, PyTOUGH, and TOUGH2 (Popineau et al., 2018).

The workflow for Hululais natural state calibration is discussed below.

As previously mentioned in Section 2.4, the geometry file and input data file are created by exporting the 3D geological combined model from Leapfrog. Before being imported to TOUGH2, the previous Leapfrog output files need to be adjusted. This adjustment was carried out with a PyTOUGH script. PyTOUGH is a Python script library, developed for automating TOUGH2 simulations (Croucher, 2015). These adjusted geometry and input files are then used in the TOUGH2 simulator. The model output will be visualized and compared to the conceptual model and measured data to determine whether the results match or not. If the calculated model does not match the measured data, the parameters in the input files need to be modified, then the simulation is re-run iteratively until a good match is reached. In some cases, when the model already matches the measured data, it is possible to update the conceptual model, and those changes can be transferred seamlessly to the reservoir model. This close coupling between the conceptual model and the numerical model reduces the effort and computational time required for updating the reservoir model significantly.

4.2 Geometry File

Leapfrog Geothermal software has a feature to generate the TOUGH2 grid blocks from the existing geological combined model. In the software, the grid is constructed interactively under its flow model plug-in. The grid dimension is designed efficiently to shorten the simulation time and yet still capture the whole system that has been defined in the conceptual model. Before creating the grid, the TOUGH2 grid has to be rotated following the orientation of the most significant faults in the system. This aims to align the faults with the model grid, which helps in assigning the reservoir parameters, such as in setting anisotropic permeability. In this case, the grid is reoriented to azimuth 37.18°, which is parallel to the NW-SE major faults in the field. Rectangular blocks are utilized in this grid model. The grid dimension is 18 km x 16 km x 5.6 km, while the surface elevation following the topography model as shown in Figure 12.

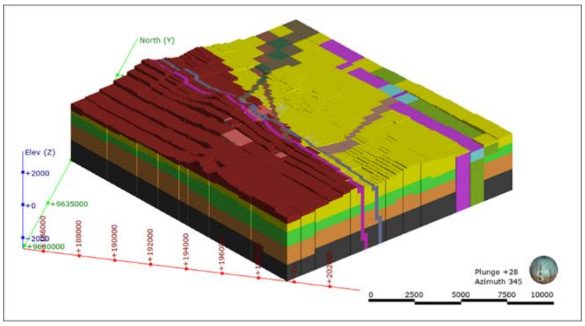

Figure 12: Hululais TOUGH2 simulation grid.

The grid model covered an elevation from 2,100 masl to -3,250 masl. The block size in the outer part starts from 1000m x 1000m x 500m and is refined down to 250m x 250m x 25m in the area of interest, where the well data exist and closer to the surface. Moreover, the grid consists of 67 layers with different thickness, as illustrated in Figure 13.

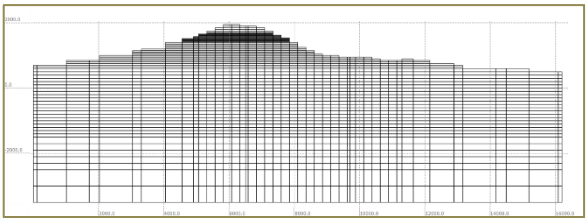

Figure 13: Vertical layers for the grid model.

4.3 Boundary Condition

4.3.1 Top Boundary

The top boundary was assigned to wet air atmospheric conditions at block "0ATM1" in the grid model due to the high annual rainfall of 327 mm/year (Pertamina Geothermal Energy, 2019a). The rainfall represents an inflow of cold water injected into the top of the model with a temperature of 27°C and enthalpy of 113 kJ/kg. The low permeability in the top surface rock (500 mD – 5,000 mD) was assigned to represent the unconsolidated soil conditions. Thus allows the infiltration and flowing of the rainwater to lower elevations following the topography.

4.3.2 Side Boundary

It assumed that no heat or mass are coming into or out of the system. Therefore, the no-flow boundary conditions were implemented at the side boundary. The side boundaries are situated far away from the production and reinjection zone.

4.3.3 Base Boundary

Hululais field is a water-dominated geothermal system. Hence the mass inflows were input at the base of the model (layer 67). These input constant mass flows were distributed in several spots corresponding to the upflow zones in the conceptual model.

Initially, the deep mass flows were set to the enthalpy of 1,500 kJ/kg and total mass flow of 63 kg/s. These deep upflows were located along the Suban Agung Hulu Fault below Mount Gedang Hululais and Mount Beriti. Thus allowing convective heat transfer in the reservoir. The input enthalpy is equivalent to a temperature of 326°C. However, the location of the input mass flows was dispersed out into several spots during the calibration process. The initial location of the input mass flow, wells, and faults are given in Figure 14.

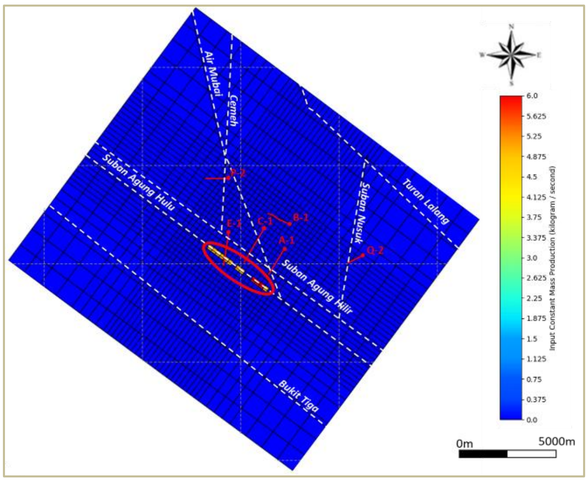

Figure 14: The initial location of input mass production (red circle), well tracks (red line), and faults (dashed white line).

4.4 Equation of State (EOS)

This model uses the EOS3 (water, air). Hence the unsaturated vadose zone could be explicitly incorporated in the model, and no water table assumptions were needed. In this EOS, the air is assumed as an ideal gas, while the total pressure is the sum of the air and water vapour partial pressure,

$$P_g = P_a + P_v.$$

Specifically, the EOS3 differs from other EOS modules of TOUGH in terms of the primary thermodynamics parameters. The primary variables of EOS3 in single-phase conditions are pressure, air mass fraction, temperature (P, X, T), while in two-phase conditions are gas phase pressure, gas saturation+10, temperature (P_g, $S_g + 10$, T) (Pruess, K. et al., 1999).

4.5 Initial State Temperature Data

The initial state temperature data was obtained from the downhole measurement during the well completion test. This temperature data reflects the initial and undisturbed condition of the reservoir before the exploitation of the geothermal resource.

Wells A1, C1, and E1 are situated in the production zone (Pertamina Geothermal Energy, 2019a). These wells are located in the upflow zone and are characterized by a high temperature of > 250°C. On the other hand, wells B1, P2, and Q2 are situated in the reinjection zone (Pertamina Geothermal Energy, 2019a), located outside the upflow zone and characterized by lower temperatures of < 215°C. The initial state temperature data is shown as a red line in Figure 15.

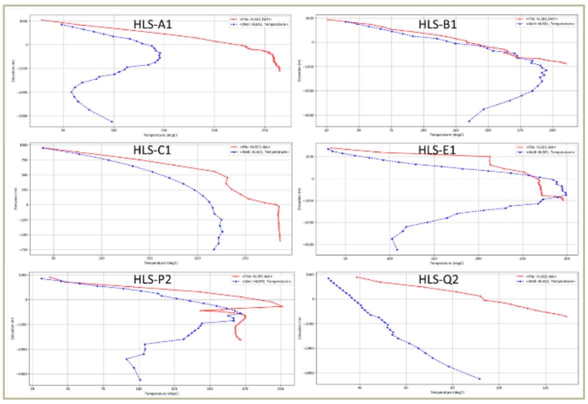

Figure 15: Graphs of the initial state temperature from the downhole measurement (red line) vs simulated temperature (blue dotted) from the first trial of the modelling.

Figure 15 shows that the error in the model is relatively high because the two curves do not fit. Therefore, the model parameters needed adjustment to decrease the error. These adjustments involve the modification of the permeability structure, redistribution of the enthalpy of the input constant mass production, and reshaping of the rock type distribution. The adjustments were made by a trial-and-error process until the best fit of the measured and calibrated temperature curve was reached.

5. RESULTS, AND ANALYSIS

5.1 Final Calibrated Model

The high-temperature wells (HLS-A1, HLS-C1, and HLS E-1) are located separately with a distance of 1 km- 1.5 km between each well. Thus, the location of the deep upflow needs to be dispersed according to the conceptual model. In this manual calibration process, the mass input has been changed from its initial setup (63 kg/s) to 102 kg/s, where the high enthalpy upflow is situated in the vicinity of the production wells as shown in Figure 16.

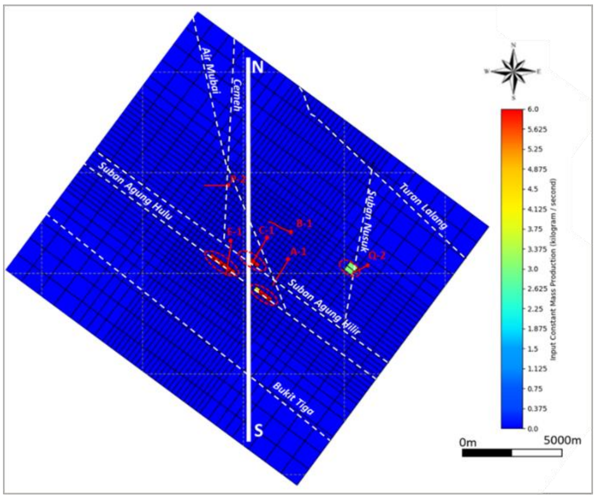

Figure 16: Final location of input mass flow (red circle), well tracks (red line), and faults (dashed white line). N-S solid white line is the slice line of the following vertical sections.

5.1.1 Final Permeability Distribution

In general, the subsurface rocks have isotropic permeability, with similar horizontal components (K1 and K2) and vertical component (K3). However, the presence of a fault gives anisotropic permeability conditions. For all rock types along the fault, the vertical permeability K3 tends to have a higher permeability than the K1 and K2 components. Figure 17 exhibits the horizontal permeability (K1) distribution of the final calibrated model.

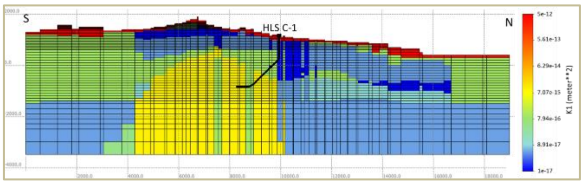

Figure 17: The S-N vertical section showing the distribution of rock permeability K1 of the final calibrated model.

5.1.2 Final Temperature Distribution

After extensive trial-and-error iterations, the initial-state model was successfully calibrated to the measured downhole temperatures. These were adjusted to achieve close to a maximum difference of 20°C between measured and simulated temperature. In this project, the average RMS error of the model is 15.1°C, while 80% of the model is within 20°C of the actual downhole data, as shown in Figure 18.

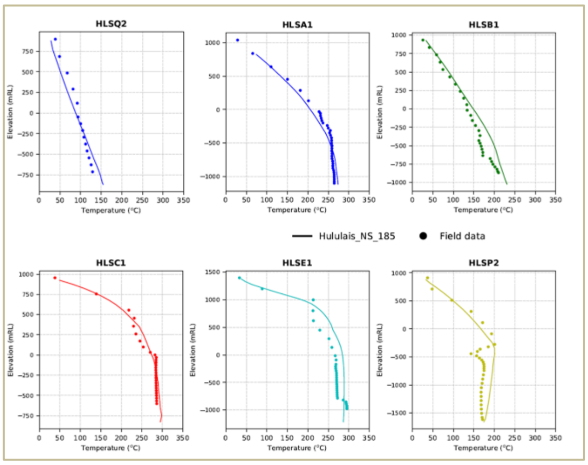

Figure 18: Graphs of final natural state temperature model (solid line) vs real downhole temperature data (dotted line).

The final temperature results range from 27°C at the top surface up to 317°C at the bottom of the model as shown in Figure 19 and 20.

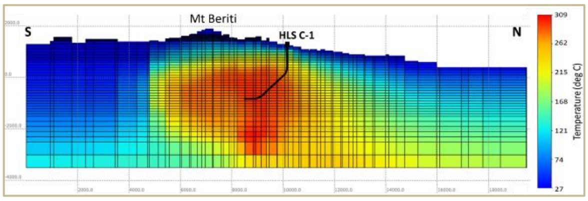

Figure 19: N-S vertical section of the natural state model, showing the subsurface temperature distribution.

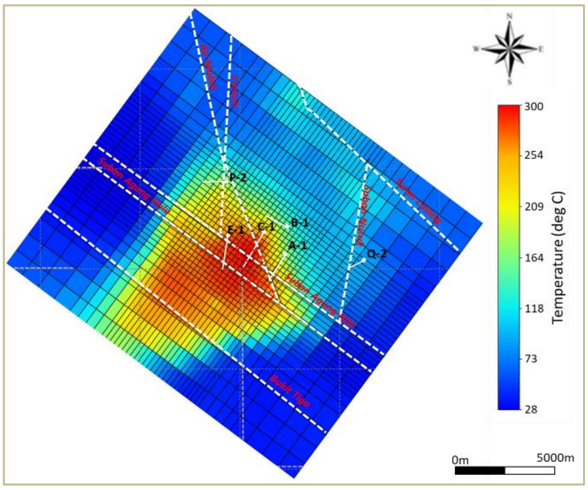

Figure 20: **Horizontal temperature distribution of the natural state model at layer 46 (- 50 masl). Well tracks are shown as solid white lines, while faults are shown as dashed white lines.**

5.2 Analysis of the Natural State Model

The reservoir permeability in the final calibrated model varies from 1 mD (tight reservoir) to 80 mD (high permeability). In contrast, the area outside the reservoir has a lower permeability, ranging from 0.01 mD to 1 mD. The clay cap and the basement rock have the lowest permeability, which are 0.01 mD and 0.05 mD, respectively. Nevertheless, the surface water table was not changed during the manual calibration. Thus, the permeability of the surface rocks remained at its initial setup value.

The temperature profile of the model shows a good correlation to the actual data as shown in Figure 18. Nevertheless, this model has the limitation of not fitting the temperature reversals due to cold water inflow especially in well HLS-P2. The convective plume beneath Mount Beriti indicates the upflow zone of the geothermal system (Figure 19). This "sweet-spot" provides a good permeability and high-temperature for the reservoir, which is already proven by wells HLS-A1, HLS-C1, and HLS E-1.

According to the conceptual model in Section 3, the Southern extent of the system is set by Bukit Tiga fault. Nonetheless, the horizontal temperature distribution of the model shows that the high-temperature zone extends further to the South West boundary (Figure 20). This anomaly is possibly due to the sparseness of the data in that area, and hence further investigation is needed to justify including this area as a geothermal prospect.

Suban Agung Hulu, and Suban Agung Hilir faults allow the upward flow of the high-temperature water and form the liquid-dominated reservoir as well as the sulphate water and fumaroles in the surface. In addition, Air Mubai and Cemeh faults are the two main structures that provide a pathway for lateral outflow of chloride-water from the reservoir to the surface.

Except for the anomaly at the Southern boundary, Figure 21 shows that the temperature distribution of the natural-state model is well correlated with the conceptual model (Figure 10). Thus, it can be claimed that the natural-state model of this field is well calibrated to the temperature profiles of the six wells, and can be used to forecast the future performance of the reservoir.

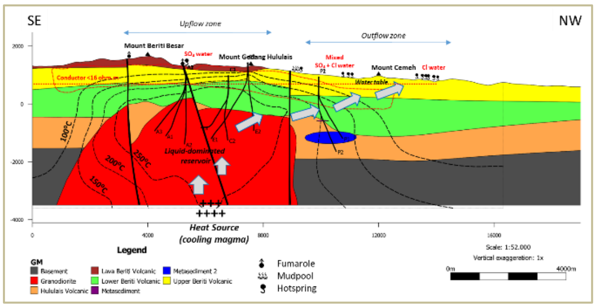

Figure 21: The subsurface temperature distribution from the numerical simulation model.

6. CONCLUSIONS AND RECOMMENDATIONS

6.1 Conclusions

The utilization of three-dimensional geophysics models (Magnetotelluric and Gravity) in Leapfrog aid the development of the geological model, especially the clay cap boundary and the shape of the granodiorite intrusion. The conceptual model was built by incorporating all available geology, geochemist and geophysics data. Hence it can represent the entire geothermal system of Hululais.

The natural-state model of Hululais shows a satisfactory agreement with the actual downhole temperature data with average RMS error 15.1°C. This good match natural-state model was yielded by the integration of the geological and conceptual model with the numerical reservoir modelling.

6.2 Recommendations

The current geological model was built from the lithology that observed from the drilling cuttings. In order to comply with the necessities of reservoir modelling, the rock types in the geological model should be preferably made as detailed as possible. Hence, it is recommended to assign more rock types in the geological model by incorporating the detailed surface geological map. Moreover, it is recommended to re-calibrate the current natural state model to the latest initial state temperature from all 24 wells data in the field to improve the model.

REFERENCES

Bambang Budiardjo, Djoko Hantono, Heni Agus, & Nugroho. (2001). Geochemical characterization of thermal waters inhululais geothermal prospect. Paper presented at the *Stanford Geothermal Workshop.*

Croucher, A. (2020). *Waiwera user guide* (1.2.1 ed.). Auckland: The University of Auckland.

Cumming, W. (2009). Geothermal resource conceptual models using surface exploration data. Paper presented at the *Thirty-Fourth Workshop on Geothermal Reservoir Engineering Stanford University, Stanford, California.*

Geothermex. (2016). *Reservoir model of the hululais geothermal field sumatra, indonesia.* Unpublished manuscript.

Kamah, Y., Palmelay, A. C., Raharjo, I. B., Thamrin, M. H., Hartanto, D. B., Silaban, M. S., & Sasradipoera, S. D. (2015). Successful exploration campaign and to be developed in hululais geothermal field, bengkulu, indonesia Paper presented at the *World Geothermal Congress.*

Koestono, H., Prasetyo, I. M., Nusantara, V. D. M., Thamrin, M. H., & Kamah, M. Y. (2015). Hydrothermal alteration mineralogy of well pad C, hululais geothermal field, bengkulu, indonesia Paper presented at the *World Geothermal Congress.*

Milicich, S. D., Pearson-Grant, S., Alcaraz, S., White, P. A., & Tschritter, C. (2018). 3D geological modelling of the taupo volcanic zone as a foundation for a geothermal reservoir model. *New Zealand Journal of Geology and Geophysics, 61*(1), 79-95. doi:10.1080/00288306.2017.1407346

Nusantara, V. D. M., Prasetyo, I. M., Thamrin, M. H., & Siahaan, E. E. (2017). 3d geological modelling : An advanced method to build geological baseline model in hululais geothermal prospect, bengkulu, indonesia Paper presented at the *New Zealand Geothermal Workshop.*

Pertamina Geothermal Energy. (2013). *Geological map of hululais.* Unpublished manuscript.

Pertamina Geothermal Energy. (2017b). *Hululais concession area map.* Unpublished manuscript.

Pertamina Geothermal Energy. (2019a). *Geochemistry update of hululais field.* Unpublished manuscript.

Pertamina Geothermal Energy. (2019b). *Subsurface review of hululais field.* Unpublished manuscript.

Popineau, J., O'Sullivan, J., O'Sullivan, M., Archer, R., & Williams, B. (2018). An integrated leapfrog/TOUGH2workflow for a geothermal production modelling. Paper presented at the *African Rift Geothermal Conference.*

Pruess, K., Oldenburg, C. M., & Moridis, G. J. (1999). *TOUGH2 user's guide version 2*. Berkeley: Earth Sciences Division, Lawrence Berkeley National Laboratory University of California, Berkeley, California 94720.

Sisminardi, Y. (2019). *The 3D geological model and natural state reservoir simulation of hululais geothermal field, bengkulu, indonesia.* Auckland: The University of Auckland.

Yeh, A., Croucher, A. E., & O'Sullivan, M. J. (2013). Tim – yet another graphical tool for tough2. Paper presented at the *New Zealand Geothermal Workshop.*